

Continuous Generation of Volumetric Images During Treatment Using kV Images and an External Respiratory Surrogate

Matthieu Lafrenière,^{1, a)} Nitin Mahadeo,¹ John Lewis,² Joerg Rottmann,³ and Christopher L. Williams¹

¹⁾Brigham and Women's Hospital, Dana-Farber Cancer Institute, Harvard Medical School

²⁾University of California, Los Angeles

³⁾Paul Scherrer Institute

(Dated: December 15, 2024)

Purpose: During radiation therapy, respiratory motion can lead to inter- and intra-fraction variations in patient anatomy, which may result in discrepancies between the planned and the delivered dose. Continuous knowledge of a patient's three-dimensional anatomy is required to fully assess the dosimetric impact of this motion, and would also enable treatment adaptation to account for any deviations in delivered dose. However, current clinical imaging techniques do not provide sufficient information to fully reconstruct 3D anatomy in real time on current clinical linear accelerators. We present a technique that combines information obtained during treatment on a standard clinical accelerator with a patient-specific motion model to generate continuous volumetric imaging that can serve as a basis for improved delivered dose calculation and adaptive radiotherapy.

Methods: A patient-specific motion model is constructed by performing principal component analysis (PCA) on displacement vector fields (DVF) created by deformably registering images of each phase of a pre-treatment four-dimensional computed tomography (4DCT) scan. During treatment, planar kV images are acquired at a maximum rate of 1/3 Hz, and the position of an external surrogate is continuously monitored. Volumetric images are reconstructed for each kV image acquisition by optimizing the PCA weights of the motion model to match the acquired planar kV image. A correlation between these PCA weights and surrogate kinetics enables continuous generation of a patient's 3D anatomy throughout treatment delivery.

Results: Performance of the algorithm was evaluated using 10 different digital eXtended CArdiac-Torso (XCAT) phantom datasets that provide a full ground truth anatomy. The XCAT phantoms were programmed to move in accordance with real 3D tumor trajectories measured using fluoroscopy of fiducial markers implanted in patients undergoing thoracic radiotherapy. Phantoms were generated every 0.2 seconds, and simulated kV images were generated every 3 seconds for image-based PCA model reconstruction. An external surrogate signal was recorded during the patient treatments (independent of the XCAT phantoms), and was used to generate the correlation model and produce 3D images every 0.2 seconds. Using digital phantom datasets with an average duration of 155.8 seconds, and comparing to the ground truth 3D tumor positions and volumetric images, three-dimensional tumor positions were reconstructed with an average root mean square error (RMSE) of 1.47 mm, and an average 95th percentile 3D positional error of 2.80 mm.

Conclusions: We demonstrate that a correlation model using kV imaging and an external respiratory surrogate to drive a PCA motion model can enable continuous generation of volumetric images of patient anatomy. This method is novel in that it utilizes imaging-based information to drive the motion model from observations of the internal anatomy, and enables near continuous 3D image generation without requiring continuous kV imaging. The information required for this technique can be provided by standard clinical linear accelerators, overcoming a major obstacle to the clinical implementation of image-based motion modeling techniques. The three-dimensional images produced with this technique can be used for treatment verification and calculating delivered dose in the presence of irregular respiratory motion, providing an important tool for adaptive radiotherapy.

PACS numbers: 87.57.-s, 87.57.N-, 87.57.nf

Keywords: Respiratory Motion Modeling, Continuous Volumetric Image Generation, Deformable Image Registration (DIR), Principal Component Analysis (PCA), External Respiratory Surrogate

I. INTRODUCTION

Respiratory motion is an outstanding challenge for radiation therapy treatments of many thoracic and ab-

dominal malignancies. This motion may result in organ

displacements of several centimeters, particularly in the superior-inferior (SI) direction^{1,2}. The respiratory motion is three-dimensional and non-rigid, affecting both the target lesion(s) as well as adjacent organs at risk, potentially causing deviations in the planned dose (target underdosage and increased dose to normal tissues)¹⁻⁴.

In typical clinical practice, accounting for organ motion relies on the use of 4DCT⁵ to define an internal target volume that encompasses the target motion. However, in standard 4DCT acquisition protocols, the imaging represents just one or two respiratory cycles in each region of the patient anatomy. This inherently presents a limited view of the patient's breathing pattern as it does not reflect any breath-to-breath changes in motion. This can lead to substantial uncertainties in the internal target volume derived from a 4DCT dataset⁶⁻⁹. Moreover, 4DCT images obtained during pre-treatment simulation may not represent internal patient anatomy and organ motion at the time of treatment, as the patient's breathing pattern may change in the intervening time^{10,11}.

Respiratory motion modeling techniques can be used to overcome some of the limitations of traditional 4DCT-based techniques, enabling improved 3D localization of target lesions and surrounding normal tissues¹²⁻¹⁶. Often, these patient-specific motion-models are created with information available prior to radiotherapy treatment, such as 4DCT¹⁶⁻¹⁹, 4DCBCT^{20,21}, or an external surrogate signal²². Deformable image registration (DIR) can be performed between the 3D images of each respiratory phase to produce a set of 3D displacement vector fields (DVF) that describe the respiratory motion in these scans.

A simplified model of the motion-induced deformations can be created by using a dimensionality-reduction technique, such as PCA, which allows the full DVF to be described as a linear combination of a small subset of vector fields. The entire 3D representation of a patient's anatomy at an arbitrary respiratory state can then be generated using only a small number of model parameters. Other information, such as lung tidal volume and airflow¹⁹, or an external respiratory surrogate^{15,22-25} can also be incorporated in the model.

3D fluoroscopic image generation is a technique that uses a patient-specific respiratory motion model in combination with 2D x-ray projection images acquired during treatment to reconstruct a full 3D volume¹¹. Parameters of the motion model are determined using an iterative optimization procedure in which a digitally reconstructed radiograph (DRR) of the modeled patient anatomy is compared with the acquired image, and the model parameters are then adjusted for an optimal match.

Previous motion modeling-based approaches have demonstrated that planar kV or MV images^{11,20,21,26,27}, as well as external surrogate signals^{22,28}, can be used independently to generate volumetric images. However, these techniques have limitations that can pose challenges for clinical implementation. For kV image-based techniques, the image acquisition frame rate is impacted

by the potential for excess imaging dose as well as machine constraints (e.g. the Varian TrueBeam platform limits in-treatment kV imaging to a rate of 1/3 Hz in clinical mode), which may result in images being acquired too infrequently to fully capture the motion during each breath. The use of MV portal images is also limited due to the small and complex apertures used with modulated treatments. For external surrogate-based techniques, the correlation between the surrogate signal and internal patient anatomy can change over time²⁹⁻³¹.

We present a technique that combines periodic triggered kV images with an external respiratory surrogate to drive a patient-specific motion model built from a pre-treatment 4DCT scan. This method is novel in that it combines image-derived model fitting with a continuous external surrogate signal, providing a new capability of generating continuous 3D volumetric information based on internal anatomy while at the same time requiring only limited kV imaging (minimizing additional imaging dose). This technique addresses many limitations of previous motion modeling techniques and enables high time-resolution 3D image generation using information that is available on current clinical treatment machines and often already acquired as part of current clinical treatments.

II. METHODS AND MATERIALS

This technique extends prior work that generates 3D images based on single planar kV images^{11,27} or external surrogate signals²², and establishes a framework that uses information from both approaches through a correlation model.

II.A. Modified digital XCAT phantom with realistic breathing from measured patient data

The overall accuracy of a time-varying volumetric image generation technique can be difficult to assess with clinically acquired data due to the lack of a "ground truth" volume to compare the generated image against. To address this issue, we use the hybrid digital eXtended CArdiac-Torso (XCAT) phantom³²⁻³⁴ seen in fig. 1. This phantom incorporates realistic anatomy³⁵ for which a ground truth is unambiguously defined, and also allows for customized irregular breathing profiles^{36,37}. This technique has been developed and used previously in our group^{11,20-22,27,38,39}, and has proved useful in quantitatively assessing the accuracy of the 4D image generation over a variety of patient-simulated conditions.

The tumor motion trajectories that were used to generate the XCAT phantoms were acquired with the Mitsubishi Real Time Radiation Therapy (RTRT) system at the Radiation Oncology Clinic at the Nippon Telegraph and Telephone Company Hospital in Sapporo, Hokkaido, Japan^{29-31,40,41}. A fluoroscopic x-ray system was used to obtain stereoscopic images to localize 1.5 mm gold fiducial markers implanted in lung tumors of

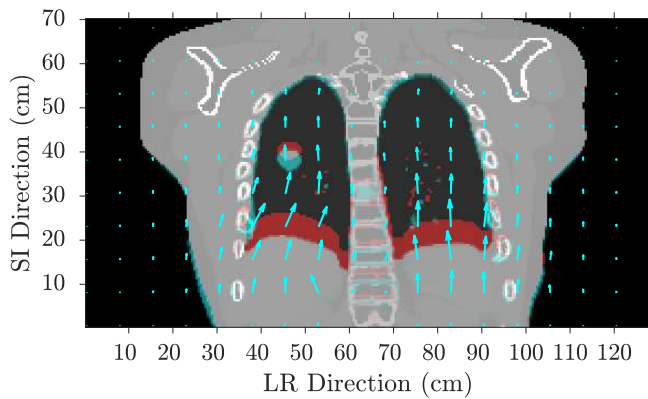


Figure 1 Example digital XCAT phantom reference image (red) overlaid with a reconstructed image from an inhale respiratory phase (cyan) of phantom #5, showing the tumor and diaphragm moving inferiorly. The reconstructed displacement vector field between the reference and reconstructed image is also shown (cyan arrows).

patients receiving radiotherapy. Digital XCAT phantoms were generated for each measured tumor motion trace. The simulated tumors were modeled as 2 cm diameter spheres whose centroid moves in accordance with the tumor motion measured using the RTRT system. The breathing motion of the XCAT phantom is controlled by the diaphragm displacement and anterior motion of the ribs, and these parameters were varied to reproduce the observed tumor motion. The remainder of the anatomy is moved and displaced according to the deformation model within the XCAT software, which can be nonlinear.

In addition to the stereoscopically-acquired tumor positions, the RTRT system also contained an external respiratory surrogate that reported the position of the patient’s abdomen at a rate of 30 Hz^{40,41}. The synthetic XCAT images produced in this study are thus independent from the external surrogate information being drawn from the RTRT dataset.

Ten XCAT phantom sets were generated from 9 separate patients (two separate datasets came from the same patient on different treatment days). An open source graphical user interface for the XCAT software was used to facilitate the creation of images based on true respiratory signals⁴². Phantoms were created with an intrinsic resolution of 2 mm in the left-right (LR) and anterior-posterior (AP) directions, and 2.5 mm in the superior-inferior (SI) direction. The total number of voxels per image is $256 \times 256 \times 140 = 9,175,040$ (LR, AP, SI). The XCAT images were produced every 0.2 second, and for each patient the entire available respiratory trace was used, which varied between 46.7 seconds and 292.0 seconds.

A training dataset was produced for each XCAT set consisting of 10 images approximately distributed over the first breathing cycle in the respiratory trace, replicating the information that would be available to train a

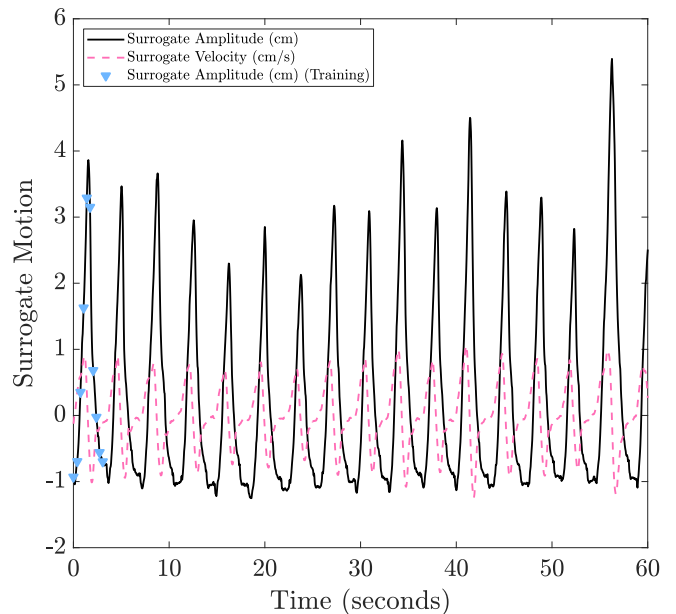


Figure 2 First 60 seconds of the respiratory trace from phantom #5 showing the external surrogate amplitude (plain black line), the surrogate velocity (dashed magenta line) and the time points chosen for generating the simulated 4DCT training phantoms (cyan triangles) used for creating the motion model.

motion model from a 4DCT simulation (empty cyan triangles in fig. 2). These “4DCT” XCAT images are spaced every 0.4 seconds for a total of 4 seconds, similarly to previous studies on 4DCT motion modeling using the digital XCAT phantom^{11,27,43}, and providing a proxy for the information available at each slice location in a clinical 4DCT or 4DCBCT.

II.B. 3D fluoroscopic image generation

II.B.1. PCA based respiratory motion model.

Each respiratory phase of the digital XCAT phantom training 4DCT set was deformably registered to a peak-exhale reference image from the same dataset using a GPU-accelerated double force demons algorithm⁴⁴ with the α parameter fixed to 2.0. A patient-specific motion-model was then constructed by performing PCA on the DVFs obtained with the registration, and retaining only the most important eigenvectors. DVFs describing the respiratory motion can typically be well represented by a linear combination of 2 to 3 PCA eigenvectors^{11,13,15,18,22,24,27,43,45–48}.

$$\mathbf{DVF} = \overline{\mathbf{DVF}} + \sum_{n=1}^N w_n(t) \mathbf{u}_n, \quad (1)$$

where $\overline{\mathbf{DVF}}$ is the mean DVF, \mathbf{u}_n is the n^{th} basis eigenvector, $w_n(t)$ is the time dependent weighting coefficient (also called PCA eigenvalue, or PCA weight) of the n^{th} PCA mode, and N is the total number of PCA

modes that are used for motion modeling. Three coefficients were used to build the respiratory motion models for this work.

II.B.2. Optimization-based 3D fluoroscopic image generation.

A 3D image can be produced from a single planar x-ray image by using a forward iterative reconstruction (FIR) process to optimize the weights $w_n(t)$ in the PCA respiratory motion model to best match the observed projection image. A simulated x-ray projection can be produced by applying a projection matrix, \mathbf{P} , to a realization of the patient's 3D anatomy, \mathbf{f} , as $\mathbf{P} \cdot \mathbf{f}$. The patient anatomy image, \mathbf{f} , is created by deforming a reference image, \mathbf{f}_0 , with a displacement vector field $\mathbf{DVF}(w)$ determined by the weights. The optimal representation of a patient's anatomy is then determined through a minimization procedure:

$$\min_w J(w) = \min_w \|\mathbf{P} \cdot \mathbf{f}(\mathbf{DVF}(w), \mathbf{f}_0) - \lambda \cdot \mathbf{x}\|_2^2, \quad (2)$$

where \mathbf{x} is the planar image acquired during treatment delivery, λ is a parameter defining the relative pixel intensity between the simulated and acquired projection images, and $J(w)$ is a cost function representing the L2-norm (squared least squares) error between the simulated and acquired planar x-ray image. A version of gradient descent is used to minimize the cost function $J(w)$ (eq. (2)). A detailed description of the PCA coefficients optimization can be found in the work of Li *et al.*^{43,46}. A schematic representation of this process is shown in fig. 3. This process is implemented in a GPU-accelerated framework so that it can be performed in real time.

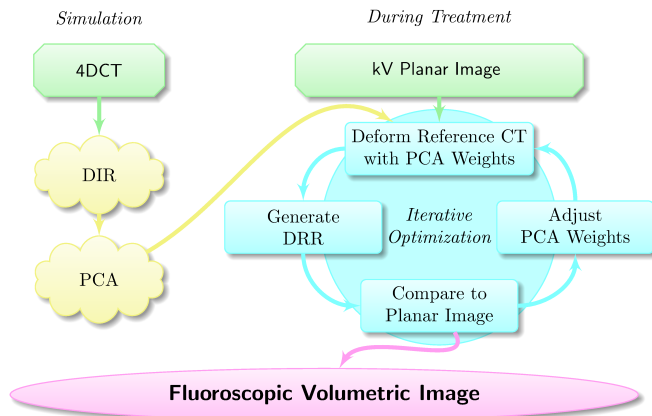


Figure 3 Forward iterative reconstruction (FIR) procedure for estimating time-varying volumetric images from single x-ray projections. In this work, a method was developed to use an external respiratory surrogate to generate volumetric images in the 3-second time interval elapsed between each acquired planar kV image.

II.B.3. Continuous volumetric image generation with an external surrogate respiratory trace.

During radiotherapy treatments, it may not be possible or desirable to acquire kV images continuously due to imaging dose or machine limitations (the TrueBeam LINACs in our clinic are limited to acquiring in-treatment kV images every 3 seconds). Thus, the framework presented in fig. 3 is extended to continuously generate 3D images in the time interval between each kV image acquisition. To accomplish this, we use the information provided by an external respiratory surrogate to estimate the PCA weights in the motion model during the inter-image time interval. This is a non-invasive, non-ionizing modality that provides the amplitude of a patient's abdominal motion with high time resolution (30 Hz).

A linear correlation model is developed between the PCA weights, and the displacement and velocity of the surrogate signal. These surrogate characteristics have been shown to be complementary in characterizing respiratory motion^{22,49}. For each kV image acquisition, the weight of each PCA mode, w_n , is determined by the procedure described in section II.B.2, and the correlation model is established:

$$w_n(t) = c_n + f_n a(t) + g_n \dot{a}(t) \quad (3)$$

where $a(t)$ is the amplitude of the external surrogate signal, and $\dot{a}(t)$ is its velocity. The parameters c_n , f_n and g_n are specific to each PCA mode of each patient's motion. The linear relationship between the first principal component (w_1) and the external surrogate amplitude and velocity ($a(t)$ and $\dot{a}(t)$) is shown in fig. 4, and is represented by the fitting surface. The first PCA component has the most importance and primarily drives the motion model, as seen in figs. 5 to 7. Correlation model generation is performed on a per-fraction basis because of potential inter-fraction changes in the correlation between internal and external anatomy²⁹⁻³¹.

PCA weights periodically reconstructed with the FIR process and PCA weights continuously generated with the correlation model are shown as a function of the external surrogate amplitude for phantom dataset #5 in fig. 5. The same PCA weights, but as a function of the external surrogate velocity, are shown in fig. 6. Finally, the PCA weights as a function of time are shown in fig. 7.

II.C. Evaluation criteria

The tumor localization error is evaluated with the 95th percentile and the RMSE between the tumor centroid location in the reconstructed volumetric images and the ground truth volumetric images. The tumor localization error is estimated in the LR, AP, and SI directions, as well as an absolute 3D positional difference, which provides a geometric measure of the reconstruction accuracy.

As a benchmark for comparison, the FIR process was also performed every 0.2 seconds, to simulate continu-

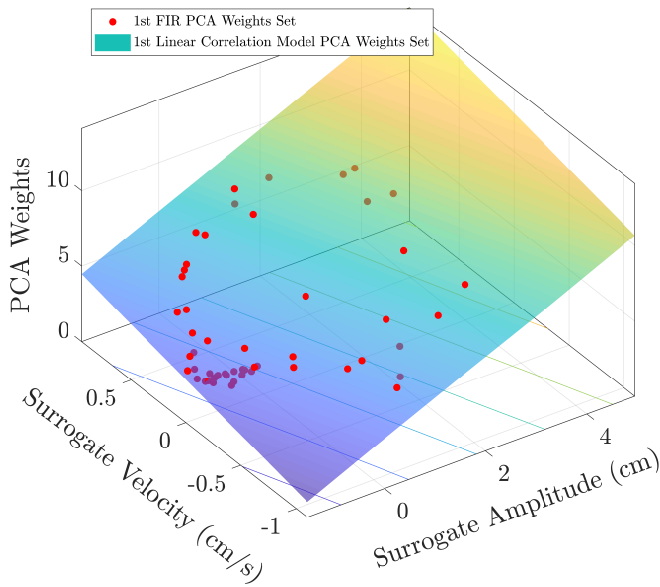


Figure 4 The weights of the first principal component of phantom dataset #5 plotted as a function of the external surrogate amplitude and velocity. The linear correlation model is represented by the fitting surface.

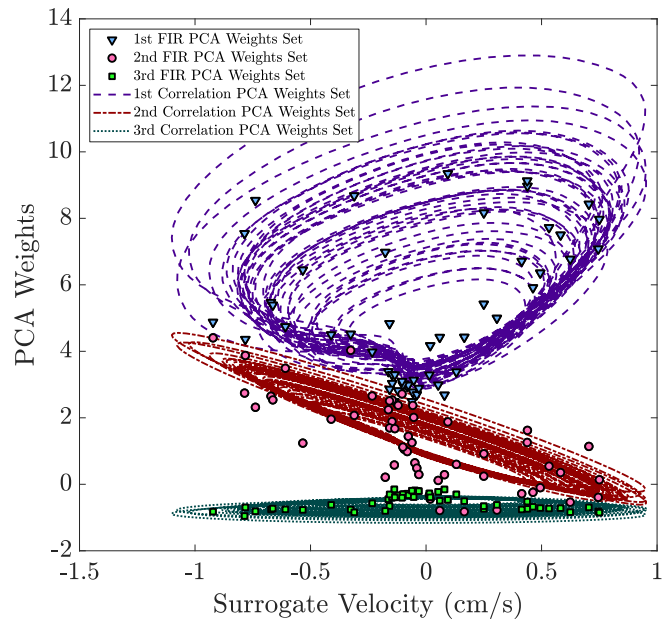


Figure 6 Three PCA weights sets created from kV images (markers) and generated with the correlation model (lines) as a function of the external surrogate velocity for phantom dataset #5.

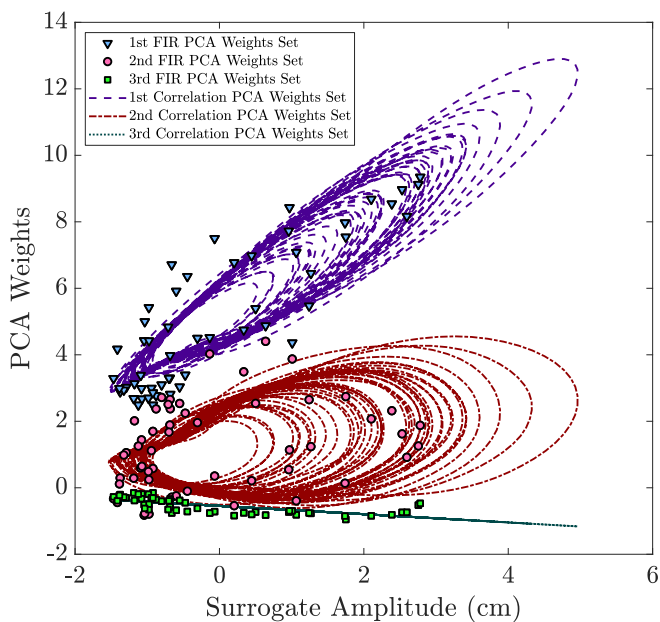


Figure 5 Three PCA weights sets created from kV images (markers) and generated with the correlation model (lines) as a function of the external surrogate amplitude for phantom dataset #5.

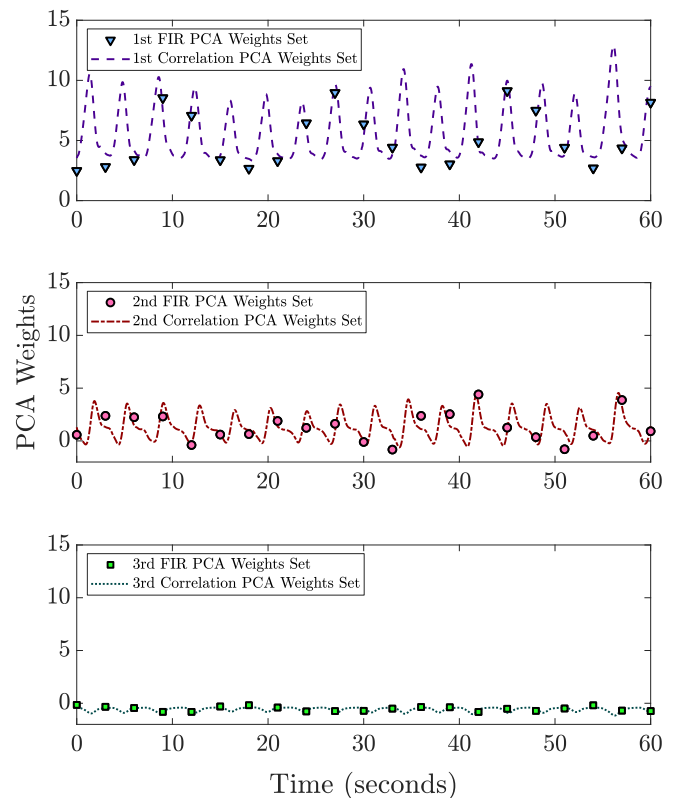


Figure 7 Three PCA weights sets created from kV images (markers) and generated with the correlation model (lines) as a function of time (phantom dataset #5). The simulated kV image rate used in the motion model for reconstruction is 1/3 Hz. The first PCA component has the dominant motion contribution.

ous kV fluoroscopy for generating motion model reconstructions. Comparing these results to the correlation model (which uses imaging every 3 seconds) allows the accuracy of the correlation method to be assessed in the context of the overall performance of the image-based motion modeling techniques.

III. RESULTS

The correlation method's performance was evaluated by comparing the position of the tumor centroid in reconstructed images to the tumor centroid position in the ground truth phantom images for each dataset. Simulated kV images were computed every 3 seconds to match the acquisition rate of current radiotherapy clinical systems. The image-based fitting procedure described in section II.B.2 was used to generate periodic PCA weights, and continuous correlation model PCA weights were determined using the full external surrogate respiratory trace.

Using the correlation model, three-dimensional reconstructions were computed every 0.2 seconds over the entire trace duration. The average trace length was 155.8 seconds long (ranging from 46.7 to 292.0 seconds). The motion in the datasets was primarily in the SI direction, and the average 3D motion amplitude was 1.7 cm. An example trace of the ground truth 3D tumor motion compared with the reconstructed 3D tumor motion is shown in fig. 8.

The accuracy of the 3D reconstruction for each phantom dataset is summarized in table I. The average 95th percentile 3D error between correlation model-generated volumetric images and ground truth volumetric images was 2.80 mm, and the RMSE was 1.47 mm (results averaged over 10 different phantom datasets). On average, tumor positions reconstructed using the correlation model method were within 3 mm of the ground truth position 94.6% of the time, and below 5 mm 99.1% of the time. A plot of the cumulative 3D differences in tumor location between the ground truth and the correlation model for all generated images from dataset #5 is shown in fig. 10. Comparison of the full volumetric ground truth and correlation model generated images gives a NRMSE of 97.83% (refer to table I).

A baseline accuracy for the image-based reconstruction method was assessed by performing the FIR process every 0.2 seconds to simulate near-continuous kV acquisition. This kV-based motion modeling technique was characterized by an average 95th percentile accuracy of 1.58 mm for the three dimensional tumor position reconstruction, and an average RMSE of 0.94 mm. This shows that the tumor position reconstruction obtained with the FIR process is better than a millimeter. When comparing the ground truth and FIR generated volumetric images, the NRMSE is 98.2% (refer to table I).

IV. DISCUSSION

This method provides a new way to continuously generate 3D images throughout a radiotherapy treatment by establishing a correlation model between motion model PCA weights determined from kV images (using information from the internal anatomy) and an external surrogate signal. This technique uses data that are often already available during treatments on conventional lin-

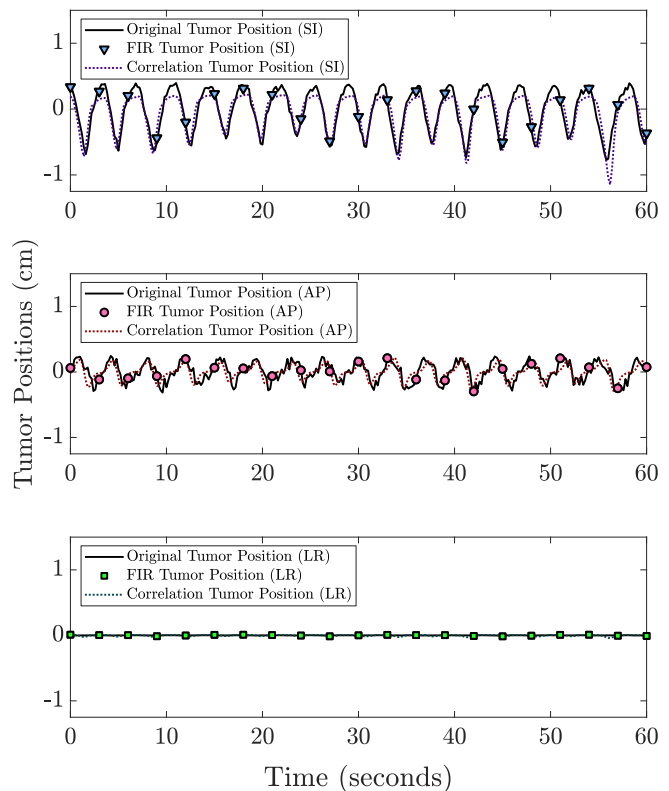


Figure 8 ground truth tumor positions in the LR, AP and SI directions (plain black lines), alongside those created by the FIR algorithm (markers) and by the correlation model (non-continuous colored lines) (phantom dataset #5). The simulated kV image rate used in the motion model for reconstruction is 1/3 Hz. The main contribution to respiratory motion comes from the SI direction.

ear accelerators, and obviates the need to capture kV images at a high frame rate in order to accurately perform motion model-based 3D reconstruction.

The correlation model used in this work differs from other techniques that have used internal-external correlation^{30,50-60} in that it relates both the amplitude and the velocity of the surrogate to PCA deformation vector fields in the motion model (as opposed to correlating surrogate amplitude and target position). Consequently this technique tracks both tumor motion and also determines the deformation of the entire patient's anatomy, including nearby organs at risk. The model can also be updated based on observed internal anatomy as more kV images are acquired. Additionally, as this technique uses information from the entire kV image (as opposed to just the tumor region), it does not suffer from limitations on tumor size or distance to other nearby structures that can often confound image-based tumor tracking techniques⁶¹. As the *cine* 3D images produced by this method are generated from deformations of a reference 4DCT planning image, they are inherently co-registered with known deformations. The DVFs produced by the motion model can then be used to calculate and accumulate the delivered dose to the patient, providing a mechanism to compute the full delivered

XCAT Dataset	Length (seconds)	3D tumor position reconstruction under 1 mm (%)		3D tumor position reconstruction under 3 mm (%)		3D tumor position reconstruction under 5 mm (%)		3D tumor position reconstruction 95 th P (mm)		3D tumor position reconstruction RMSE (mm)		3D image comparison NRMSE (%)	
		FIR	COR	FIR	COR	FIR	COR	FIR	COR	FIR	COR	FIR	COR
1	61.8	59.9	36.6	94.2	83.2	96.8	93.5	3.21	6.31	1.46	2.64	98.29	97.96
2	75.6	93.9	65.5	98.4	96.0	99.2	98.1	1.11	2.75	0.99	1.87	98.73	98.38
3	46.7	75.1	76.4	100	99.1	100	100	1.51	2.22	0.85	0.96	96.87	95.96
4	141.3	100	98.0	100	100	100	100	0.35	0.86	0.21	0.45	98.73	98.62
5	161.4	95.7	54.6	100	97.6	100	99.8	0.97	2.62	0.54	1.36	98.22	97.65
6	141.3	100	61.3	100	98.9	100	100	0.48	2.29	0.29	1.16	98.65	98.56
7	169.1	49.9	45.3	94.7	100	100	100	2.02	2.39	1.16	1.39	98.39	98.37
8	223.8	59.1	65.9	100	99.5	100	100	1.91	2.12	1.09	1.07	97.90	97.47
9	245.0	13.5	26.8	97.4	73.8	100	100	2.93	3.90	2.13	2.40	97.97	97.79
10	292.0	71.1	48.3	100	98.4	100	100	1.35	2.50	0.80	1.38	97.82	97.48
Average	155.8	71.8	57.9	98.5	94.6	99.6	99.1	1.58	2.80	0.94	1.47	98.16	97.83

Table I Three dimensional tumor positions over an average respiratory trace of 155.8 seconds are reconstructed with a 95th percentile averaged over 10 datasets of 1.58 mm with FIR, and 2.80 mm with the correlation model (COR). The average root mean square error averaged over 10 datasets between ground truth and FIR generated volumetric images is 0.94 mm with FIR, and the average RMSE between ground truth and the correlation (COR) generated volumetric images is 1.47 mm. The voxel by voxel intensity volumetric image comparison yields a normalised root mean squared error of 98.16% with FIR, and a NRMSE of 97.83% with the correlation model (COR).

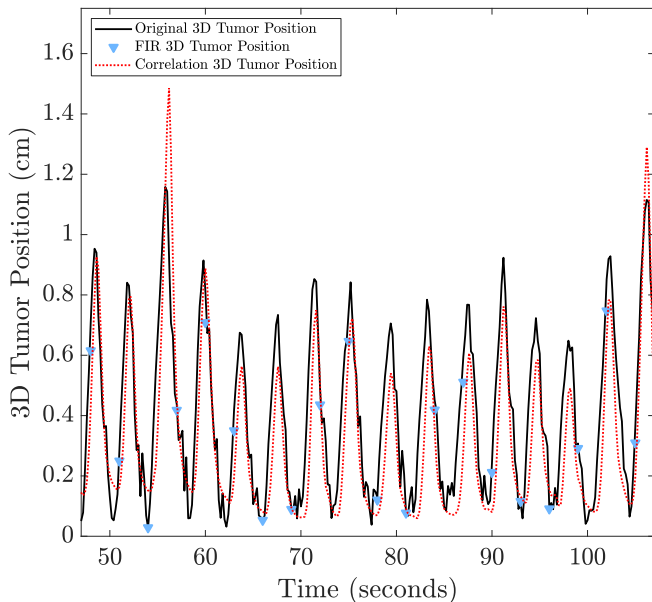


Figure 9 The ground truth three dimensional tumor position (plain cyan curve) is displayed alongside the correlation model reconstructed 3D tumor position (dashed red curve), and the position determined from performing the FIR process on 1/3 Hz kV images (cyan triangles) (phantom dataset #5), illustrating the ability of the technique to reconstruct motion with high time resolution, even in the presence of irregular breathing.

dose in the presence of respiratory motion.

The 3D tumor position is reconstructed with an average RMSE of 1.47 mm, which compares favorably with other similar tracking methods that use both images and external surrogates (e.g. the Xsight Lung Tracking System, which has a precision of 1.5 mm to 4 mm^{56,57,62–64}). Performing volumetric image recon-

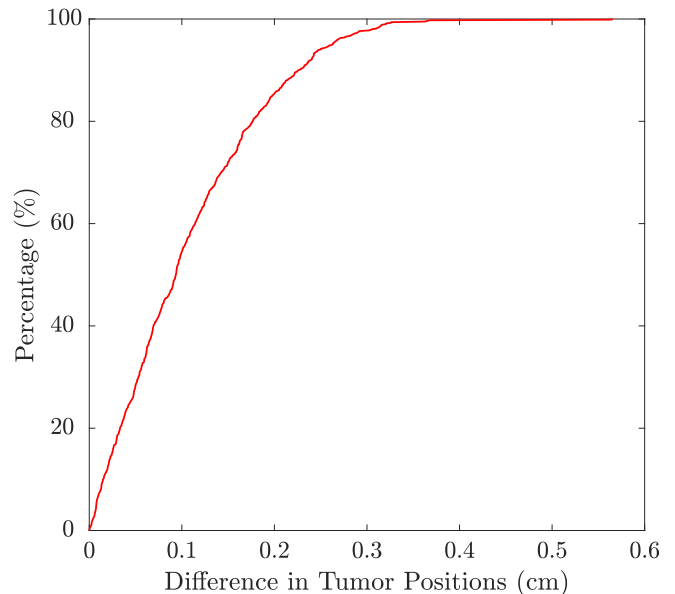


Figure 10 Cumulative 3D difference between the ground truth tumor positions, and the tumor positions reconstructed using the correlation model (phantom dataset #5). For this dataset, the 95th percentile difference is 2.62 mm, and the RMSE of the tumor position reconstruction is 1.36 mm. When averaged over all datasets, the tumor position difference is below 2.80 mm for 95% of the data, and below 3 mm for 94.6% of the data.

struction using high frame rate kV images (0.2 second interval) yields an average RMSE of 0.94 mm in the tumor position reconstruction. Comparing to the results of the correlation model with a 3-second imaging interval shows that although the accuracy of the reconstruction decreases, the overall performance degradation (0.53 mm in the RMSE) is small compared to typ-

ical respiratory motion amplitudes. Voxelwise comparison of both the FIR-generated and correlation model-generated volumetric images to the ground truth images yields similar NRMSE, indicating good agreement between the methods in regions outside of the tumor.

The use of simulated digital phantoms enabled a detailed analysis of the full 3D accuracy of this technique, however, it also constitutes a limitation. Although the phantoms used in this study match clinically observed respiratory patterns, the internal anatomic details of the phantom are not fully representative of a real patient. This can impact the performance of the deformable image registration as well as the fitting of the PCA weights from kV images. Additionally, physical effects such as scatter or imaging artifacts are not included in the image projection process. A full validation of this technique will require evaluation with clinically acquired kV images. However, the ground truth comparison provided by this phantom study provides important preliminary data that can be used to better understand those future results. As prior studies have already demonstrated the performance of kV-based PCA motion modeling techniques using clinical patient images, we believe the results of this analysis should generalize to clinically acquired imaging data.

It is important to note that the XCAT phantoms used in this study are derived from tracking patient tumor motion during radiotherapy treatments. Consequently, the motion patterns observed (respiratory rate, amplitude, variability) are true representations of the types of motions that can occur during patient treatments. Furthermore, the external surrogate signal used for generating the correlation model was also recorded during treatment (not derived from the XCAT phantoms). This means that the results presented in this work include any changes in internal-external correlation.

The method presented in this work relies on a motion model built using DVFs generated from DIR between phases of a pre-treatment planning image set. Any uncertainties in these vector fields will be reflected in the motion model, and thus the accuracy of the DIR method places a limit on the precision of the generated images. Although a demons algorithm⁴⁴ was used in this work, the method presented can use any DIR technique. Using registration techniques that may more accurately incorporate the biomechanical properties of respiratory motion may lead to better results^{65,66}. Incorporating models developed from pre-treatment 4DCBCT²¹ rather than a planning 4DCT may also improve the accuracy of the method by compensating for day-to-day changes in patient respiratory motion that may differ from the reference model.

This work uses a basic linear correlation model, and the results could be improved by developing a correlation model using a more advanced function or method, such as machine learning, neural networks^{67,68}, nearest neighbor method⁶⁹ or fuzzy logic⁶³. Moreover, the linear correlation model could be adjusted after every im-

age acquisition so that the continuous correlation model-generated PCA weights are forced to agree with the periodic planar kV image-derived PCA weights.

In this study, the correlation model built for each dataset comes from the entire length of the respiratory trace. However, the correlation between the internal and external anatomy can potentially change with time²⁹, and implementing a time-adaptive correlation model that only uses a portion of the trace may improve accuracy. Additional improvements such as including the uncertainty in the FIR generation process in the model fitting, or smoothly adjusting the correlation model to agree with the FIR results at the observed imaging time-points may also enhance accuracy, and will be investigated in future work.

The volumetric images produced with this technique are inherently coregistered, as they are reconstructed by determining a DVF relative to a reference image. This allows these image sets to be used for computing accumulated delivered dose during the fraction, which may show discrepancies from what was originally planned (especially if the planning doses were calculated on e.g. the average intensity projection image). Through this process, underdosage of the target or overdosage of critical structures can be identified, and corrected in subsequent fractions through plan adaptation.

V. CONCLUSION

We have demonstrated a new technique for continuously generating dynamic volumetric images of patient anatomy using periodic planar kV images in combination with an external respiratory surrogate that is suitable for use with current standard clinically available linear accelerator systems. The performance of the method was assessed with 10 digital XCAT phantoms that included real patient breathing patterns and enabled a comparison with ground truth tumor motion, demonstrating tumor localization to better than 1.47 mm on average. Correlation model generated volumetric images were reconstructed with a NRMSE of 97.83% compared to the XCAT phantom ground-truth volumetric images.

This method is novel in its combination of image-based PCA motion modeling and external surrogate kinematics for volumetric image reconstruction. It enables motion modeling to be performed with high time resolution on data that can be acquired on current clinical linear accelerators (and in some cases is already routinely acquired in clinical practice), without additional kV imaging. The 3D images produced using this technique can be used to calculate delivered dose in the presence of respiratory motion for thoracic and abdominal treatments. This will provide an important tool for treatment verification, delivered dose calculation, and adaptive radiotherapy.

ACKNOWLEDGMENTS

We would like to thank Dr. Seiko Nishioka of the Department of Radiology, NTT Hospital, Japan, Dr. Hiroki Shirato of the Department of Radiation Medicine, Hokkaido University, Japan, and Dr. Ross Berbeco of Brigham & Women's Hospital for sharing the patient tumor position dataset with our group.

This project was supported through a Master Research Agreement with Varian Medical Systems, Inc.

In memory of Guillaume Barlet.

REFERENCES

- ^{a)} **Corresponding Author:** Matthieu Lafrenière, PhD
E-Mail: Matthieu.Lafreniere@DFCI.Harvard.edu
- ¹Keall P. J., Mageras G. S., Balter J. M., et al. The management of respiratory motion in radiation oncology report of AAPM Task Group 76a) *Medical Physics*. 2006;33:3874-3900.
 - ²Korremans S. S.. Image-guided radiotherapy and motion management in lung cancer *The British Journal of Radiology*. 2015;88:20150100. PMID: 25955231.
 - ³Jiang S. B.. Radiotherapy of Mobile Tumors *Seminars in Radiation Oncology*. 2006;16:239 - 248. Innovative Technologies in Radiation Therapy.
 - ⁴Vedam S. S., Keall P. J., Kini V. R., Mostafavi H., Shukla H. P., Mohan R.. Acquiring a four-dimensional computed tomography dataset using an external respiratory signal *Physics in Medicine & Biology*. 2003;48:45.
 - ⁵Rietzel E., Pan T., Chen G. T. Y.. Fourdimensional computed tomography: Image formation and clinical protocol *Medical Physics*. 2005;32:874-889.
 - ⁶St. James S., Mishra P., Hacker F., Berbeco R. I., Lewis J. H.. Quantifying ITV instabilities arising from 4DCT: a simulation study using patient data *Physics in Medicine & Biology*. 2012;57:L1.
 - ⁷Sarker J., Chu A., Mui K., et al. Variations in tumor size and position due to irregular breathing in 4DCT: A simulation study *Medical Physics*. 2010;37:1254-1260.
 - ⁸Cai J., McLawhorn R., Read P. W., et al. Effects of breathing variation on gating window internal target volume in respiratory gated radiation therapy *Medical Physics*. 2010;37:3927-3934.
 - ⁹Cai J., Read P. W., Sheng K.. The effect of respiratory motion variability and tumor size on the accuracy of average intensity projection from fourdimensional computed tomography: An investigation based on dynamic MRI *Medical Physics*. 2008;35:4974-4981.
 - ¹⁰St. James S., Seco J., Mishra P., Lewis J. H.. Simulations using patient data to evaluate systematic errors that may occur in 4D treatment planning: A proof of concept study *Medical Physics*. 2016;40:091706.
 - ¹¹Mishra P., Li R., St. James S., et al. Evaluation of 3D fluoroscopic image generation from a single planar treatment image on patient data with a modified XCAT phantom. *Physics in Medicine & Biology*. 2013;58:841.
 - ¹²Fassi A., Schaerer J., Fernandes M., Riboldi M., Sarrut D., Baroni G.. Tumor Tracking Method Based on a Deformable 4D CT Breathing Motion Model Driven by an External Surface Surrogate *International Journal of Radiation Oncology*Biophysics*. 2014;88:182 - 188.
 - ¹³Zhang Q., Hu Y.C., Liu F., Goodman K., Rosenzweig K. E., Mageras G. S.. Correction of motion artifacts in conebeam CT using a patientspecific respiratory motion model *Medical Physics*. 2010;37:2901-2909.
 - ¹⁴Lewis J. H., Li R., Watkins W. T., et al. Markerless lung tumor tracking and trajectory reconstruction using rotational cone-beam projections: a feasibility study *Physics in Medicine & Biology*. 2010;55:2505.
 - ¹⁵Zhang Q., Pevsner A., Hertanto A., et al. A patientspecific respiratory model of anatomical motion for radiation treatment planning *Medical Physics*. 2007;34:4772-4781.
 - ¹⁶Sohn M., Birkner M., Yan D., Alber M.. Modelling individual geometric variation based on dominant eigenmodes of organ deformation: implementation and evaluation *Physics in Medicine & Biology*. 2005;50:5893.
 - ¹⁷Hertanto A., Zhang Q., Hu Y.C., Dzyubak O., Rimner A., Mageras G. S.. Reduction of irregular breathing artifacts in respiration-correlated CT images using a respiratory motion model *Medical Physics*. 2012;39:3070-3079.
 - ¹⁸Li R., Lewis J. H., Jia X., et al. On a PCA-based lung motion model *Physics in Medicine & Biology*. 2011;56:6009.
 - ¹⁹Low D. A., Parikh P. J., Lu W., et al. Novel breathing motion model for radiotherapy *International Journal of Radiation Oncology*Biophysics*. 2005;63:921 - 929.
 - ²⁰Cai W., Hurwitz M., Williams C. L., et al. 3D delivered dose assessment using a 4DCTbased motion model *Medical Physics*. 2015;42:2897-2907.
 - ²¹Dhou S., Hurwitz M., Mishra P., et al. 3D fluoroscopic image estimation using patient-specific 4DCBCT-based motion models *Physics in Medicine & Biology*. 2015;60:3807.
 - ²²Hurwitz M., Williams C. L., Mishra P., et al. Generation of fluoroscopic 3D images with a respiratory motion model based on an external surrogate signal *Physics in Medicine & Biology*. 2015;60:521.
 - ²³McClelland J. R., Hughes S., Modat M., et al. Inter-fraction variations in respiratory motion models *Physics in Medicine & Biology*. 2011;56:251.
 - ²⁴Staub D., Docef A., Brock R. S., Vaman C., Murphy M. J.. 4D Conebeam CT reconstruction using a motion model based on principal component analysis *Medical Physics*. 2011;38:6697-6709.
 - ²⁵Cho Byungchul, Suh Yelin, Dieterich Sonja, Keall P. J.. A monoscopic method for real-time tumour tracking using combined occasional x-ray imaging and continuous respiratory monitoring *Physics in Medicine & Biology*. 2008;53:2837.
 - ²⁶Harris W., Wang C., Yin F. F., Cai J., Ren L.. A Novel method to generate on-board 4D MRI using prior 4D MRI and on-board kV projections from a conventional LINAC for target localization in liver SBRT *Medical Physics*. 2018;45:3238-3245.
 - ²⁷Mishra P., Li R., Mak R. H., et al. An initial study on the estimation of timevarying volumetric treatment images and 3D tumor localization from single MV cine EPID images *Medical Physics*. 2014;41:081713.
 - ²⁸Li R., Mok E., Han B., Koong A., Xing L.. Evaluation of the geometric accuracy of surrogate-based gated VMAT using intrafraction kilovoltage x-ray images *Medical Physics*. 2012;39:2686-2693.
 - ²⁹Wu H., Zhao Q., Berbeco R. I., Nishioka S., Shirato H., Jiang S. B.. Gating based on internal/external signals with dynamic correlation updates *Physics in Medicine & Biology*. 2008;53:7137.
 - ³⁰Kanoulas E., Aslam J. A., Sharp G. C., et al. Derivation of the tumor position from external respiratory surrogates with periodical updating of the internal/external correlation *Physics in Medicine & Biology*. 2007;52:5443.
 - ³¹Berbeco R. I., Nishioka S., Shirato H., Chen G. T. Y., Jiang S. B.. Residual motion of lung tumours in gated radiotherapy with external respiratory surrogates *Physics in Medicine & Biology*. 2005;50:3655.
 - ³²Segars P. W., Sturgeon G., Mendonca S., Grimes J., Tsui B. M. W.. 4D XCAT phantom for multimodality imaging research *Medical Physics*. 2010;37:4902-4915.
 - ³³Segars P. W., Tsui B., Lalush D., Frey E., King M., Manocha D.. Development and application of the new dynamic NURBS-based Cardiac-Torso (NCAT) phantom. *Journal OF Nuclear Medicine*. 2001;42:23.
 - ³⁴Segars P. W., Lalush D. S., Tsui B. M. W.. Modeling respiratory mechanics in the MCAT and spline-based MCAT phantoms *IEEE Transactions on Nuclear Science*. 2001;48:89-97.
 - ³⁵Spitzer V. M., Whitlock D. G.. The visible human dataset: The anatomical platform for human simulation *The Anatomical Record*. 1998;253:49-57.
 - ³⁶Berbeco R. I., Mostafavi H., Sharp G. C., Jiang S. B.. Towards fluoroscopic respiratory gating for lung tumours without radiopaque markers *Physics in Medicine & Biology*. 2005;50:4481.
 - ³⁷Pankaj M., St. James S., Segars P. W., Berbeco R. I., Lewis J. H.. Adaptation and applications of a realistic digital phantom based on patient lung tumor trajectories *Physics in Medicine & Biology*.

- 2012;57:3597.
- ³⁸Cai W., Dhou S., Cifter F., et al. 4D cone beam CT-based dose assessment for SBRT lung cancer treatment *Physics in Medicine & Biology*. 2016;61:554.
- ³⁹Williams C. L., Mishra P., Seco J., et al. A mass-conserving 4D XCAT phantom for dose calculation and accumulation *Medical Physics*. 2013;40:071728.
- ⁴⁰Shirato H., Shimizu S., Kitamura K., et al. Four-dimensional treatment planning and fluoroscopic real-time tumor tracking radiotherapy for moving tumor *International Journal of Radiation Oncology*Biography*Physics*. 2000;48:435 - 442.
- ⁴¹Shirato H., Shimizu S., Kunieda T., et al. Physical aspects of a real-time tumor-tracking system for gated radiotherapy *International Journal of Radiation Oncology*Biography*Physics*. 2000;48:1187 - 1195.
- ⁴²Myronakis M. E., Cai W., Dhou S., et al. A graphical user interface for XCAT phantom configuration, generation and processing *Biomedical Physics & Engineering Express*. 2017;3:017003.
- ⁴³Li R., Lewis J. H., Jia X., et al. 3D tumor localization through real-time volumetric xray imaging for lung cancer radiotherapy *Medical Physics*. 2011;38:2783-2794.
- ⁴⁴Gu X., Pan H., Liang Y., et al. Implementation and evaluation of various demons deformable image registration algorithms on a GPU *Physics in Medicine & Biology*. 2010;55:207.
- ⁴⁵Zhang Y., Yang J., Zhang L., Court L. E., Balter P. A., Dong L.. Modeling respiratory motion for reducing motion artifacts in 4D CT images *Medical Physics*. 2013;40:041716.
- ⁴⁶Li R., Jia X., Lewis J. H., et al. Realtime volumetric image reconstruction and 3D tumor localization based on a single xray projection image for lung cancer radiotherapy *Medical Physics*. 2010;37:2822-2826.
- ⁴⁷Vaman C., Staub D., Williamson J., Murphy M. J.. A method to map errors in the deformable registration of 4DCT images *Medical Physics*. 2010;37:5765-5776.
- ⁴⁸Zeng R., Fessler J. A., Balter J. M.. Estimating 3-D Respiratory Motion From Orbiting Views by Tomographic Image Registration *IEEE Transactions on Medical Imaging*. 2007;26:153-163.
- ⁴⁹Zhao T., Lu W., Yang D., et al. Characterization of free breathing patterns with 5D lung motion model *Medical Physics*. 2009;36:5183-5189.
- ⁵⁰He P., Li Q., Xiao G., Wang X., Ouyang S., Liu R.. Effect of respiratory guidance on internal/external respiratory motion correlation for synchrotron-based pulsed heavy-ion radiotherapy *Australasian Physical & Engineering Sciences in Medicine*. 2018;41:713-720.
- ⁵¹Wu H., Besemer A., Lu M.. Dynamic correlation of synchronized internal tumor and external skin respiratory motion for image guided lung cancer radiation treatment *International Journal of Computers and their Applications*. 2014;21:14-23.
- ⁵²Fayad H., Pan T., Clement J. F., Visvikis D.. Technical Note: Correlation of respiratory motion between external patient surface and internal anatomical landmarks *Medical Physics*. 2011;38:3157-3164.
- ⁵³Liu C., Alessio A., Kinahan P.. Respiratory motion correction for PET/CT with internal-external motion correlation *Journal of Nuclear Medicine*. 2010;51:78.
- ⁵⁴Nishioka S., Nishioka T., Kawahara M., et al. Exhale fluctuation in respiratory-gated radiotherapy of the lung: A pitfall of respiratory gating shown in a synchronized internal/external marker recording study *Radiotherapy and Oncology*. 2008;86:69 - 76.
- ⁵⁵Beddar A. Sam, Kainz Kristofer, Briere Tina Marie, et al. Correlation between internal fiducial tumor motion and external marker motion for liver tumors imaged with 4D-CT *International Journal of Radiation Oncology*Biography*Physics*. 2007;67:630 - 638.
- ⁵⁶Sayeh S., Wang J., Main W.T., Kilby W., Maurer C.R.. *Respiratory Motion Tracking for Robotic Radiosurgery*. Springer 2007.
- ⁵⁷Fu D., Kahn R., Wang B., et al. *Xsight Lung Tracking System: A Fiducial-Less Method for Respiratory Motion Tracking*. Springer 2007.
- ⁵⁸Ionascu D., Jiang S. B., Nishioka S., Shirato H., Berbeco R. I.. Internal-external correlation investigations of respiratory induced motion of lung tumors *Medical Physics*. 2007;34:3893-3903.
- ⁵⁹Korremans S., Mostafavi H., Le Q-T, Boyer A.. Comparison of respiratory surrogates for gated lung radiotherapy without internal fiducials *Acta Oncologica*. 2006;45:935-942.
- ⁶⁰Gierga D. P., Brewer J., Sharp G. C., Betke M., Willett C. G., Chen G. T. Y.. The correlation between internal and external markers for abdominal tumors: Implications for respiratory gating *International Journal of Radiation Oncology*Biography*Physics*. 2005;61:1551 - 1558.
- ⁶¹Rubio C., Morera R., Hernando O., Leroy T., Lartigau S. E.. Extracranial stereotactic body radiotherapy. Review of main SBRT features and indications in primary tumors *Reports of Practical Oncology & Radiotherapy*. 2013;18:387 - 396. Selected Papers Presented at the XVII SEOR Congress, Vigo, 1821 June 2013.
- ⁶²Yang Z.-Y., Chang Y. T., Liu H.-Y., Liu G., Li Q.. Target margin design for real-time lung tumor tracking stereotactic body radiation therapy using CyberKnife Xsight Lung Tracking System in *Scientific Reports* 2017.
- ⁶³Torshabi A. E., Riboldi M., Fooladi A. A. I., Mosalla S. M. M., Baroni G.. An adaptive fuzzy prediction model for real time tumor tracking in radiotherapy via external surrogates *Journal of Applied Clinical Medical Physics*. 2013;14:102-114.
- ⁶⁴Kilby W., Dooley J. R., Kuduvalli G., Sayeh S., Maurer C. R. Jr.. The CyberKnife Robotic Radiosurgery System in 2010 *Technology in Cancer Research & Treatment*. 2010;9:433-452. PMID: 20815415.
- ⁶⁵Samavati N., Velec M., Brock K. K.. A hybrid biomechanical intensity based deformable image registration of lung 4DCT *Physics in Medicine & Biology*. 2015;60:3359.
- ⁶⁶Brock K. K.. Results of a Multi-Institution Deformable Registration Accuracy Study (MIDRAS) *International Journal of Radiation Oncology*Biography*Physics*. 2010;76:583 - 596.
- ⁶⁷Seregni M., Pella A., Riboldi M., Orecchia R., Cerveri P., Baroni G.. Real-time tumor tracking with an artificial neural networks-based method: A feasibility study *Physica Medica*. 2013;29:48 - 59.
- ⁶⁸Isaksson M., Jalden J., Murphy M. J.. On using an adaptive neural network to predict lung tumor motion during respiration for radiotherapy applications *Medical Physics*. 2005;32:3801-3809.
- ⁶⁹Zhang J., Huang X., Shen Y., Chen Y., Cai J., Ge Y.. Nearest Neighbor Method to Estimate Internal Target for Real-Time Tumor Tracking *Technology in Cancer Research & Treatment*. 2018;17:1533033818786597. PMID: 30081745.